Femtosecond spectroscopy of cluster anions: insights into condensed-phase phenomena from the gas-phase

Jan R. R. Verlet

Received 9th November 2007
First published as an Advance Article on the web 27th November 2007
DOI: 10.1039/b700528h

Ultrafast spectroscopy allows chemical and physical processes to be observed on time-scales faster than the nuclear motion within molecules. This *tutorial review* explores how such experiments, and specifically time-resolved photoelectron spectroscopy on gas-phase cluster anions, provide a molecular-level understanding of the processes that are normally associated with condensed-phase dynamics.

1. Introduction

One of the basic goals of physical chemistry is to gain a fundamental understanding of chemical structure and dynamics on a molecular level and a wide range of spectroscopic techniques have been developed over several decades to approach this goal. As most chemistry and virtually all biology occurs in the condensed-phase, it is desirable to study and ultimately understand chemical dynamics in such environments. However, it is also this environment that greatly complicates matters. Specifically, spectral features are broadened and the overall dynamics can be dramatically altered by the presence of, for example, a solvent, such that it is often difficult to distinguish between solvent-induced dynamics or processes of the nascent solute. Gas-phase experiments circumvent these problems by investigating a gaseous ensemble of molecules, sufficiently dilute that there are no interactions with the surroundings. In doing so, one can gain unprecedented insight and detail into the structure and dynamics of isolated molecules and gas-phase spectroscopy and dynamics have played an undisputed role in our current understanding of molecular dynamics. However, ignoring bulk interactions often means that the isolated species is an inappropriate model for the same entity in a condensed-phase, because many bulk mechanisms are inoperable in the isolated molecule. So, we have come full-circle and seek to study molecular dynamics in the condensed-phase directly. An attractive alternative is provided by gas-phase clusters, which are isolated aggregates of atoms or molecules. They present a unique environment in which the benefits associated with gas-phase spectroscopy are largely retained – that is, they are isolated from the surroundings except for those atoms or molecules purposely aggregated and these specifically introduce condensed-phase interactions and phenomena in a systematic manner. As such, clusters have been clichéd as forging a bridge between the gas- and condensed-phases. In this *tutorial review*, we hope to provide the reader with an overview on the appropriateness of this cliché with a specific focus on molecular dynamics studied using ultrafast spectroscopic tools.

As aggregates, clusters can range from just a few to several thousand constituent atoms or molecules and their composition can be tailored to mimic most extended systems. As examples, one may make a cluster containing Au_n atoms to simulate bulk gold; or one may simulate a solution by clustering a solute ion to solvent molecules. Anionic clusters are particularly prevalent as microscopic model solutions and to investigate solvation dynamics. More generally anions are ubiquitous in nature and in chemical and biological processes. Additionally, anionic clusters are ideal probes for bulk interactions as will be demonstrated throughout this review. Traditionally, the size-dependent evolution of both the geometric and electronic structure of clusters has been topical because this probes the transition from the isolated atom to the condensed-phase directly[1]. This is done by monitoring spectral features with size and comparing these to bulk spectra and theoretical calculations. While such frequency-domain studies can observe the onset of bulk phenomena such as electronic bands and surface plasma resonances, in general it cannot directly probe dynamical processes that become accessible with the transition to the condensed-phase. In order to probe such processes on a molecular level, one seeks to observe the dynamics in real-time. This is the premise of ultrafast spectroscopy.

With the emergence of commercial ultrafast lasers in the mid-80's, optical pulses as short as a few femtoseconds (1 fs = 10^{-15}s) enabled one to monitor nuclear motion and energy

Department of Chemistry, University of Durham, Durham, UK DH1 3LE. E-mail: j.r.r.verlet@durham.ac.uk

Jan R. R. Verlet

Jan Verlet received his MSci in chemistry from King's College London in 1999, where he also obtained a PhD in 2003. He moved to the University of California at Berkeley, where he worked as a post-doctoral fellow in the group of Professor Daniel M. Neumark. In 2006, he joined the department of chemistry at the University of Durham as a lecturer in chemical physics and is currently an EPSRC Advanced Research Fellow.

transfer within a molecule in real-time as the optical pulses are shorter than these processes. This development established an entirely new and still burgeoning field of research coined femtochemistry.[2] In its most common guise, generally referred to as pump–probe spectroscopy, an ultrafast 'pump' pulse initiates a reaction, while a delayed 'probe' pulse monitors the subsequent evolution of the system. The nature and extent of information that can be extracted from such experiments generally depends on what the probe pulse measures. For example, in the condensed-phase, a widely applied approach is to monitor the transient absorption following excitation. In the gas-phase, samples are too dilute to perform such experiments and resonance-enhanced multiphoton ionisation or laser-induced fluorescence has been commonly employed. In this review, the primary focus is on time-resolved photoelectron spectroscopy (TRPES), described in detail in the next section. It provides information concerning the energy content and flow along the entire reaction coordinate of the molecular or cluster system. The reader is referred to a comprehensive review of the application of TRPES to both neutrals and anions.[3] Ultrafast spectroscopy is specifically well-suited for cluster studies as frequency-domain measurements incur broadening due to the convergence to the bulk. In time-resolved measurements, one does not intimately care about spectral resolution because the information is contained in the dynamical evolution of spectral features.

In Section 2, femtosecond techniques applicable to studying cluster dynamics are described, with an emphasis on TRPES. In Section 3 and its subsections, specific examples of experiments that relate to a broad range of condensed-phase phenomena are described. These include: solvation dynamics; dynamics of the solvated electron; hot-electron dynamics in metals; and surface desorption dynamics. Section 4 presents a summary and outlook.

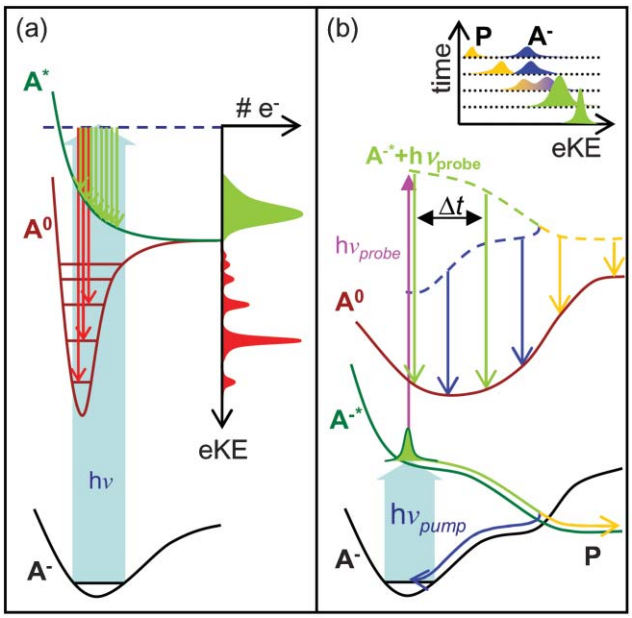

Fig. 1 Schematic diagram of the principles of (a) photoelectron spectroscopy (PES) and (b) time-resolved photoelectron spectroscopy (TRPES). In PES, anion, A^-, is photo-detached leaving the neutral in its ground state, A^0 or excited state A^*. The former produces photoelectrons with high kinetic energy (red arrows) and the latter with lower kinetic energy (green arrows). A pictorial representation of the kinetic energy distribution for a bound A^0 state and a repulsive A^* is shown in the inset. In TRPES, (b), A^- is excited to A^{-*} with a pump pulse. From this, a probe pulse photo-detaches the anion, accessing the neutral ground state, A^0. This produces electrons with kinetic energies, which depend on the time at which they were produced along the reaction coordinate, Δt, leading either to products, P (yellow arrow), or A^- ground state (blue arrow). The inset shows a pictorial representation a time-resolved photoelectron spectrum for the dynamics.

2. Anion femtosecond spectroscopy

In the gas-phase, detection schemes are restricted by the fact that the sample contains relatively few species – a situation exasperated for anions. As a result, one must resort to very sensitive techniques, typically involving the detection of a charged species, as this can be done with near-unit efficiency. In TRPES, these are photoelectrons and TRPES is a direct extension of photoelectron spectroscopy, PES, which is conceptually based on the photoelectric effect. Irradiation of a sample with light of sufficient photon energy leads to the emission of an electron from the sample. As energy must be conserved, the electron is ejected with a kinetic energy, defined as the difference between the photon energy and the initial binding energy of the electron to the sample – see Fig. 1(a). In PES, this electron kinetic energy, eKE, is measured. For the current discussion, the sample is an isolated gas-phase anion and the difference in photon energy and measured eKE, yields a vertical binding energy, defined as the difference in energy between the anionic initial state and the neutral states accessed at the geometry of the anion. The intensity of the peaks is determined by the photo-detachment cross section and Franck–Condon factors as shown in Fig. 1(a). PES has been used extensively on clusters to monitor electronic and structural transitions as the size of the cluster is increased and approaches the bulk.[1]

In its time-resolved variant, a photo-chemical or -physical process is first initiated by an ultrashort laser pulse, which excites the anion from its ground state to a non-stationary excited state (light blue arrow in Fig. 1(b)). From this excited state, a second ultrashort pulse (pink) casts the intermediate excited state energy to higher energy (dashed lines). The photoelectrons emitted are projected onto the neutral states and the resultant eKE profile of these electrons is measured (green downward arrow). This then provides direct information about the vertical binding of the electron at the time it was removed. By repeating the experiment at several pump–probe delays, Δt, represented in Fig. 1(b) by a progression of downward arrows, one builds a time-resolved map of the vertical binding energy of the system as it relaxes back to the ground state (blue path) or to some reaction product (yellow path). TRPES thus provides both temporal and spectroscopic resolution, although there always is a trade-off between these due to the uncertainty principle.

Often, however, TRPES cannot follow the dynamics to completion as there may be large differences in time-scales for various processes. For example, evaporation from a hot cluster may take nanoseconds or even microseconds. Such time scales

are generally beyond the range of a femtosecond experiment as it would require optical delay lines of several meters. To offer insight into the products formed asymptotically, ion fragment yield spectroscopy is an important companion for TRPES. In this, product yields following excitation are measured in a non-time-resolved fashion. Ion yield spectroscopy has also been extensively used in time-resolved experiments, particularly on neutrals, where one initially forms an excited state and then probes this non-stationary state by ionisation. The cations are measured by time-of-flight at various pump probe delays. In general, a decay of the signal is caused by a loss of population from the excited state due to relaxation (or reaction), although various other related probing schemes have been implemented to study specific aspects of photochemical processes. The use of mass-spectroscopy as a probe also allows one to establish the size of the neutral cluster investigated and such techniques have provided detailed insight into the dynamics of various processes such as: dissolution of acids and salts from a solvent cluster; proton-transfer reactions; solvation dynamics; to name a few. The reader is referred to a comprehensive review on femtosecond spectroscopy of clusters[4] and more generally, to volume 104, issue 4, of *Chemical Reviews*, which has been entirely devoted to femtochemistry. The focus of this *tutorial review* is, however, on TRPES of anionic species and specifically anionic clusters and in what follows, an overview of the main components of such experiments are presented.

In a typical cluster source, aggregation is promoted by rapid cooling and condensation in a supersonic expansion of a carrier gas seeded by the cluster constituents. Anion formation typically involves a plasma, generated by for example, electron or ion bombardment, laser ablation, or electric discharge. Condensation in the expansion results in a broad distribution of clusters, with an overall shape and peak that may be altered by varying the source conditions. It is, however, impossible to produce a molecular beam of a specific cluster size. As a consequence, experiments on neutral clusters have been rather difficult as the size cannot be determined prior to excitation in a straight-forward manner. In the case of charged clusters however, separation is trivial and has been done for many decades in mass-spectrometers. Thus, an experiment may be performed on a specific, predetermined cluster.

In addition to mass-selection, anions are ideal subjects for PES because of their low electron binding energies, relative to neutrals or cations. Electron detachment of an anion generally requires light in the UV range whereas VUV is necessary to ionise a neutral. The former is readily generated from a femtosecond laser system, typically using non-linear crystals. On the other hand, ionisation of neutrals commonly involves resonance enhancement through an intermediate. This leads to the restriction that resonance enhancement is only possible in a small Franck–Condon window and thus, only a small part of the reaction coordinate is probed. A further consequence is that for an anion, one can monitor not only the excited state, but often also the ground state. This is particularly informative, because it allows one to follow the energy relaxation from the excited state all the way to the ground state or products. Finally, photo-detachment does not incur stringent selection rules so that inter-system crossing to optically dark states can also be observed.

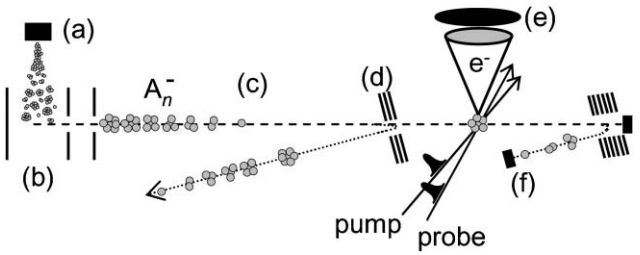

Fig. 2 Schematic representation of the main components of a time-resolved photoelectron spectrometer. A cluster source (a) produces anionic clusters, A_n^-, which are accelerated in (b) and separate in a field-free drift tube (c) by their time-of-flight. A mass-gate (d) permits only a specific mass to progress and all other clusters are deflected. This ion packet is then intersected by pump and probe femtosecond pulses and photoelectrons, e^-, are collected in the photoelectron spectrometer (e). With probe blocked, photofragments may be separated in a second mass-spectrometer and collected (f).

The main components of a vacuum system used to perform anion TRPES are shown in Fig. 2. The source, (a), as mentioned, can be one of a wide range of cluster sources. Anions are extracted, typically in a Wiley–McLaren type time-of-flight mass spectrometer,[5] (b) and (c). Time-of-flight is the natural choice because it is inherently pulsed and the arrival of the ion packet at the detection region can be synchronised to the arrival of the laser pulses. All anions in the ion beam, except for a specific anion of selected mass-to-charge ratio, may be rejected (d), leaving an ion packet of a specific anionic cluster to progress to the photoelectron spectrometer. In this region, pump and probe pulses intersect the ion packet and produce photoelectrons, which may then be detected and counted (e). Measuring the eKE can, in its simplest form, be done by extracting electrons that pass through an aperture and monitoring their time-of-flight. The drawback is that one collects only in a small solid angle and typically $<0.1\%$ of the electrons produced are collected. A more elaborate version of this is the magnetic bottle spectrometer[6], which uses a magnetic field gradient to guide the electrons out of the interaction region and into a time-of-flight tube. Near unit collection efficiency of the electrons can be achieved in this manner. A more recent addition to the arsenal has been to image the electrons using velocity-map-imaging,[7] which essentially consists of an electrostatic immersion lens that projects the velocity vectors of the expanding photoelectron cloud onto a 2D detector. The full 3D distribution of emitting electrons may be reconstructed if there is cylindrical symmetry and from this, one can not only obtain the photoelectron spectrum, but also information about the angular distribution of the emitted photoelectrons. This provides an additional dimension to TRPES and can be used to gain further insight into dynamical processes.[8] Like the magnetic bottle, collection efficiency is high and approaches unity. In parallel to the photoelectron spectrometer, one can also measure the ion yield as shown in (f) of Fig. 2.

Laser systems typically used are commercial, chirp-pulse amplified Ti:Sapphire based systems producing $\sim$1 mJ per pulse at $\sim$800 nm and 1 kHz. The high pulse energy is necessary as the photoelectron signal generated depends on the

product of both the pump and probe pulse intensities. In order to access specific excited states of interest, the pump beam can be tuneable by use of, for example, optical parametric amplifiers. The probe can be at a fixed energy, chosen to exceed the binding energy of the system. Most TRPES anion cluster experiments to date have a temporal resolution on the order of 100–200 fs.

3. Approaching condensed-phase problems with gas-phased clusters

In the spirit of a *tutorial review*, it is not the aim here to provide a full review of anion TRPES and the reader is referred to some excellent recent reviews.[3,4,9] Instead we focus on a small number of studies that are particularly representative of establishing connections to condensed-phase problems. These will include: caging of a dissociating molecule embedded in a cluster, which has direct links to bulk solvation processes; electron relaxation dynamics in water clusters, which may be related to the dynamics of the hydrated electron; ultrafast relaxation in metal clusters, in analogy to hot-electron thermalisation in bulk metals; and finally desorption from metal clusters, comparable to desorption from metal surfaces.

3.1 Solvation dynamics of I_2^-(Solvent)$_n$

In the gas-phase, dissociation of a molecule results in the products escaping each other. In contrast, in the condensed-phase, dissociation is restricted by the presence of the surroundings. This leads to various dynamical effects observed in the condensed-phase, such as caging, formation of contact pairs, and recombination.[10] Experimental evidence of such processes in clusters was first presented by the seminal work from the Lineberger group and has previously been reviewed.[11] These were based on the dissociation of I_2^- *via* the $A'^2\Pi_{g,1/2} \leftarrow X^2\Sigma_u^+$ transition, potential energy curves of which are shown in Fig. 3, which was solvated by clusters of Ar and CO_2. Ion yield experiments on $I_2^-(CO_2)_n$ and $I_2^-(Ar)_n$ show that, following dissociation of the I_2^- moiety, $I_2^-(CO_2)_{n-m}$ and $I_2^-(Ar)_{n-m}$ clusters are observed. This implies the I and I^- fragments have recombined to form I_2^- and that m CO_2 molecules and m Ar atoms have been expelled from the cluster, respectively. For $I_2^-(CO_2)_n$, the effect is first observed at $n = 4$ and becomes more prominent with increasing size, and for $n \geqslant 16$ is 100% efficient and no dissociated $I^-(CO_2)_n$ fragments can be observed in the ion yield spectrum.

In addition to this, time-resolved ion yield spectra provided details about the timescale of the processes.[12] In these elegant experiments, both pump and probe are at the same energy and are resonant with the dissociative $A'^2\Pi_{g,1/2} \leftarrow X^2\Sigma_u^+$ transition. The pump initiates the dissociation of I_2^-(Solvent)$_n$, which ultimately results in a I_2^-(Solvent)$_{n-m}$ distribution, in which the I_2^- moiety has vibrationally relaxed. At long delay, a probe pulse, also resonant with the $A'^2\Pi_{g,1/2} \leftarrow X^2\Sigma_u^+$ transition, will produce further fragmentation to form I_2^-(Solvent)$_{n-m-o}$. At pump–probe delays short compared to recombination and cooling, the internuclear separation is much larger than the equilibrium bond length of I_2^- and the probe is no longer resonant with any transition. Thus, an ion

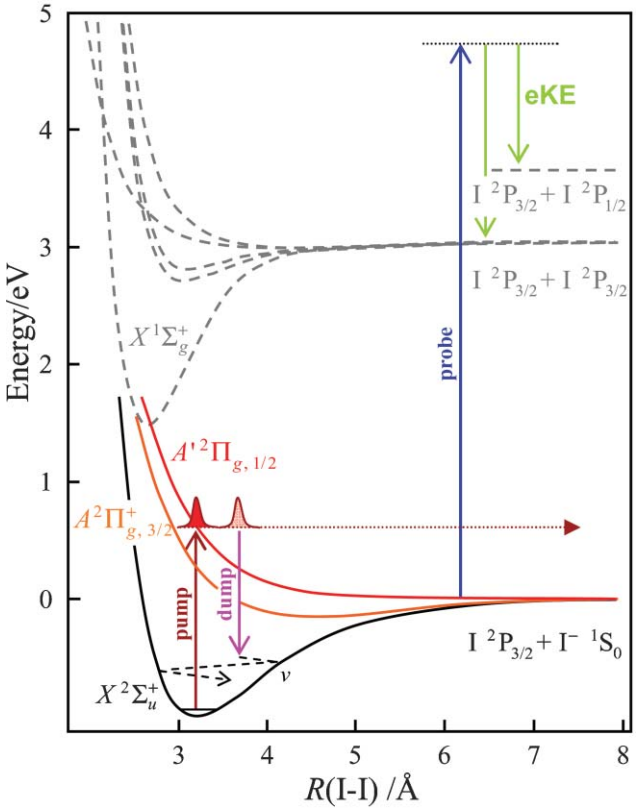

Fig. 3 Potential energy curves for the ground (black) and first two excited states (red and orange) of the I_2^- anion, and ground and low-lying I_2 neutral states (grey dashed lines). The pump pulse initiates dissociation. The probe pulse detaches the electron along the reaction coordinate and photoelectrons are emitted with electron kinetic energy, eKE (green arrows). Pump–dump excitation (see text), excites a wavepacket on the ground state of I_2^-, with average vibrational energy, v.

yield depletion in I_2^-(Solvent)$_{n-m-o}$ is observed. Recovery of this signal is then a direct measure of the recombination and vibrational cooling of I_2^- in the cluster. This is shown in Fig. 4 for a range $I_2^-(CO_2)_n$ cluster sizes.[12] These show that caging becomes more rapid with cluster size. Additionally, when compared to Ar clusters, rates are faster by two orders of magnitude, which is indicative of the stronger binding of the CO_2. Similar experiments have been performed[11] with different solvents such as OCS; different chromophores such as IBr^-; and different excitation, leading, for example to the spin–orbit excited iodine atom following the dissociation of I_2^-. All these experiments were complemented by extensive theoretical studies and provided a picture of the structures and overall dynamics.

Although the above results provide direct information about the product distribution and timescales of their formation, the probe step in these time-resolved experiments relies on a return of the wavepacket to the Franck–Condon region. In contrast, TRPES probes the entire coordinate shown in Fig. 3 and can thus also monitor the dynamics away from the Franck–Condon region. This was demonstrated by the Neumark group on the same clusters.[13,14] The results of this are shown in Fig. 5 for $I_2^-(Ar)_n$.[13] For bare I_2^-, excitation to the $A'^2\Pi_{g,1/2}$ state

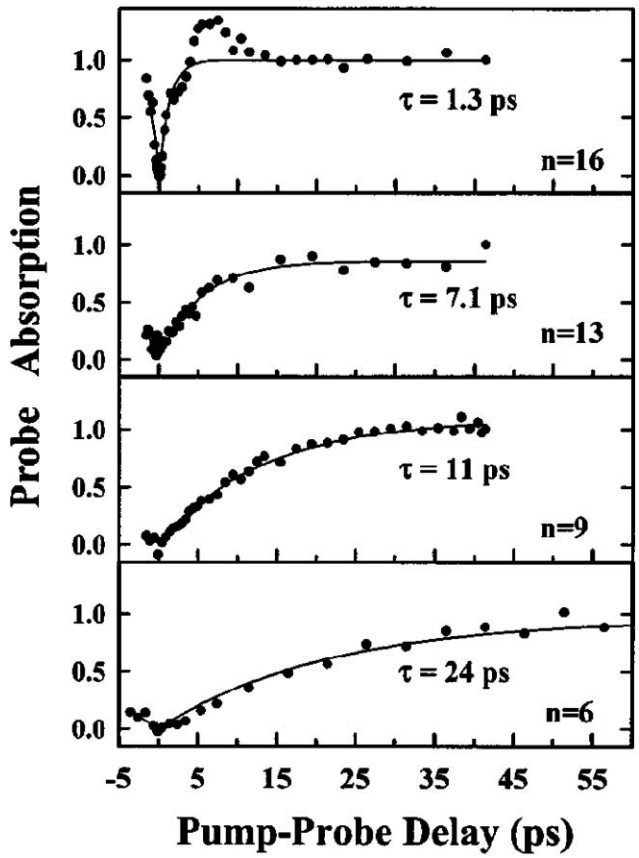

Fig. 4 Time-resolved ion yield spectra of $I_2(CO_2)_n^-$ following photodissociation of the I_2^- chromophore at 1.6 eV. The transient recovery of the signal correlates to the reformation of I_2^- in the (CO_2) cluster (see text for details). (Reproduced from ref. 12 with permission. Copyright 1997 American Institute of Physics.)

leads to prompt dissociation, which is complete in 300 fs as evidenced by the appearance of the sharp atomic photo-detachment features from I^- product, seen as B_1 and B_2 in Fig. 5(a). The doublet arises from the spin–orbit splitting of the ground neutral iodine atom. When clustered with 12 Ar atoms, Fig. 5(b), dissociation proceeds on a similar timescale and after 300 fs the dynamics look very similar to that of the unclustered I_2^-. However, several picoseconds later, new features emerge in the spectra, which are labelled as D_1, D_2, E, and F in Fig. 5. Following dissociation, caging of the $I\cdots I^-$ moiety by the Ar cluster leads to recombination, which may proceed *via* either the ground state or the electronically excited $A^2\Pi^+_{g,3/2}$ state; both converge to the same dissociation limit (see Fig. 3). For the latter, I_2^{-*} is weakly bound and photo-detachment leads to features D_1 and D_2 in Fig. 5(b). In the case of recombination *via* the ground $X^2\Sigma^+_u$ state, highly excited vibrational states are initially populated, which results in the very broad photoelectron features E and F. In Fig. 5(b), these features do not evolve any further as the Ar cluster has been evaporated and excess vibrational energy cannot be dissipated. In contrast, the dynamics for $I_2^-(Ar)_{20}$, shown in Fig. 5(c), reveal additional dynamics. Over a 200 ps timescale, feature E (and less clearly feature F) can be seen to shift towards lower kinetic energy, representative of vibrational cooling of the I_2^- and the storage of energy within the Ar cluster, which ultimately results in evaporation of the remaining Ar atoms.

Similar dynamics were observed in $I_2^-(CO_2)_n$ for clusters with $n \geqslant 6$.[14] Caging dynamics leading to recombination to form I_2^- and vibrational relaxation resulting in evaporation of CO_2 were all observed to proceed more rapidly than in the Ar case, consistent with a stronger binding solvent network able to accommodate the excess energy more efficiently. Finally, the production of a solvent-separated fragment pair, where both the fragments I and I^- are solvated but remain separated by the solvent, could also be observed for clusters with $n \geqslant 9$. In the condensed phase, these could then diffuse away.

In addition to the detail obtained through the above experiments, specific aspects of the relaxation processes may

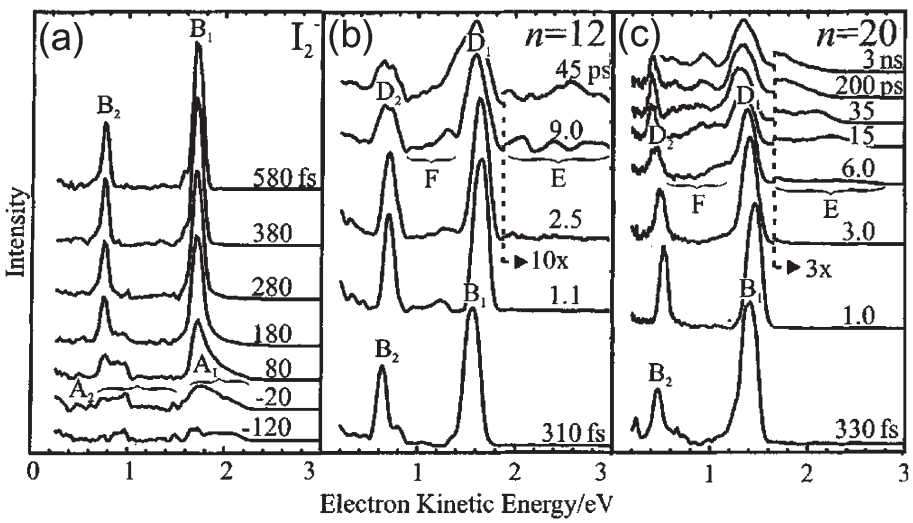

Fig. 5 Time-resolved photoelectron spectra of $I_2(Ar)_n^-$, with $n = 0$ (a), $n = 12$ (b) and $n = 20$ (c). Pump–probe delays are indicated on each trace. Features B_1 and B_2 are due to the photo-detachment form I^- – see Fig. 3. Features D_1 and D_2 correlate with photo-detachment from I_2^- reformed on the $A^2\Pi^+_{g,3/2}$ state. Feature E and F are assigned to photo-detachment from high vibrational levels in the ground state of I_2^-. (Adapted from ref. 13 with permission. Copyright 1999 American Institute of Physics.)

be investigated by careful choice of the excitation scheme. Using a two-pulse excitation, in which a pump initiates dissociation and a second 'dump' pulse forces some of the population back to the ground state, the Neumark group created vibrationally excited I_2^-. This excitation scheme is represented in Fig. 3. Using an appropriate delay and frequency for the dump-pulse, a wavepacket is formed with a well-defined average vibrational energy and this is then probed by TRPES. In this manner, details of how the vibrating chromophore loses energy in a solvent cluster can be directly observed[15]. The vibrational oscillation time was seen to decrease with time, in agreement with a lowering average vibrational energy in the anharmonic potential well of I_2^- as energy is dissipated to the cluster. It also showed rapid scrambling of the wavepacket due to dephasing from incoherent interactions with the cluster, which is a prominent bulk phenomenon and is one of the main reasons for the added complexity of dynamics in the condensed-phase.

The combination of a range of complementary experiments described above and supported by extensive theoretical modelling, reveal in detail, the intricate processes that lead to solvation, recombination and energy dissipation on a truly molecular level.

3.2. Relaxation dynamics of the hydrated electron

Most polar solvents support cavities in which an electron can be trapped. The most important of these is the hydrated electron – a ubiquitous entity of importance in various branches of chemistry and biology and central to radiation chemistry. In essence, it represents the most fundamental solute and has been coined the hydrogen atom of solution-science. However, its properties and study have by no means been as predictable as the hydrogen atom. One of these properties has been relaxation from its excited states.

In the ground state, the hydrated electron occupies a roughly spherical cavity and consequently has *s*-state character.[16] It was first identified by a strong absorption around 720 nm, which results in the excitation to the first excited states, consisting of three *p*-states supported by the cavity. The relaxation from this back to the ground state has been extensively studied in liquid water as it is an intermediate in the photo-production of the hydrated electron. Briefly, transient absorption experiments revealed three distinct timescales: 50 fs, 200–300 fs and ~1 ps time-scales.[17] These should be correlated with the expected mechanisms for relaxation. As shown in Fig. 6(a), we may expect some response of the solvent to the change in charge distribution following excitation, and hence some excited state solvation, occurring on time τ_p. Internal conversion back to the ground state must occur at some point, on a timescale τ_{ic}, producing hot ground state. This then thermalises and solvates the electron back to an equilibrated ground state, with time-constant, τ_s. The assignment of transient absorption experiments has however not been straightforward. Several models invoked to fit the data appear to provide good agreement despite being based on differing permutations of the above processes. As a result, there has been no definitive consensus about the actual relaxation mechanism.[17]

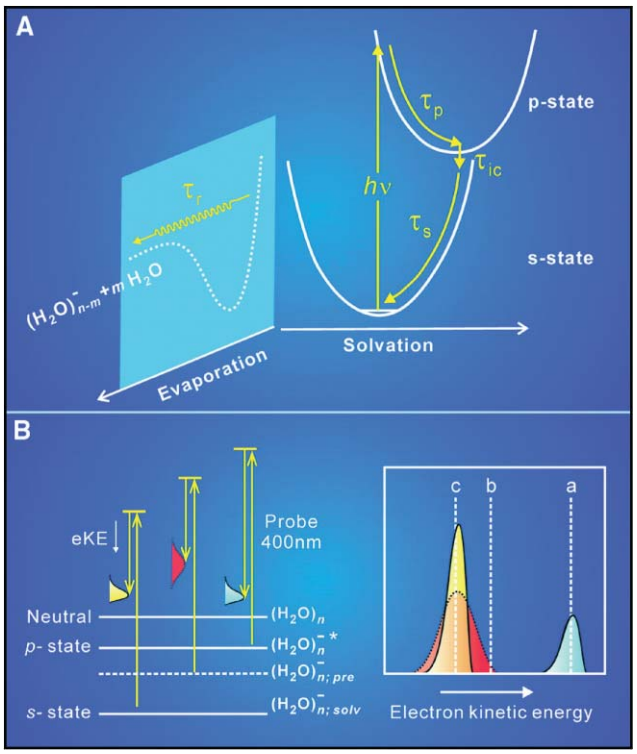

Fig. 6 (a) Schematic overview of the relaxation processes following excitation of $(H_2O)_n^-$ from the *s*-state to the excited *p*-states. Excited state solvation, internal conversion, ground-state solvation and evaporation occur on timescales: τ_p, τ_{ic}, τ_s, and τ_r, respectively. (b) Probing scheme used in experiments, following excitation. The electron kinetic energy, eKE, is indicated by the downward arrows. Photo-detachment from ground state produces a photoelectron feature at low eKE (yellow); from pre-solvated, hot ground state, a broadened feature (red); and from the excited state, a feature at higher eKE (blue). A representative photoelectron spectrum is shown in the inset. (Reproduced from ref. 19 with permission. Copyright 2004 American Association for the Advancement of Science.)

Motivated by work from the Johnson group, which had measured the absorption profile of the excess electron in water clusters and instigated the first time-resolved experiments,[18] both the Zewail and Neumark groups independently performed TRPES experiments on $(H_2O)_n^-$ clusters.[19,20] These complementary studies show that, as in the condensed-phase, three time-scales could be identified. Experiments by the Neumark group focused on the first observed timescale, while the Zewail group considered the subsequent dynamics in detail.

Fig. 7 shows the time-resolved photoelectron spectra obtained for $(D_2O)_{25}^-$ excited at 1.5 eV and probed at 3.1 eV[20] (see Fig. 6(b) for details). The probe is sufficient to remove the electron from the ground state and thus both the excited and ground state populations are monitored concurrently. The feature at highest eKE, labelled as I in Fig. 7, corresponds to the excited state and gains intensity as the probe overlaps with the pump. As the probe is delayed with respect to the pump, the integrated excited state population is observed to decay. This decay is mirrored by an increase in integrated ground state population, feature II. The concomitant rise and fall of the ground and excited state populations, respectively, is consistent with internal conversion. The lifetime

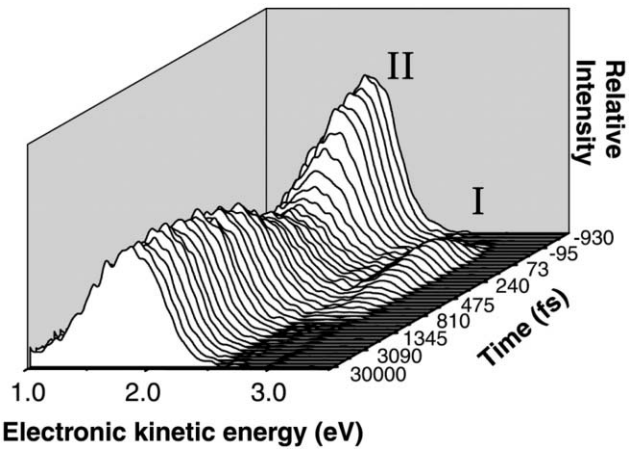

Fig. 7 Time-resolved photoelectron spectra for $(D_2O)_{25}^-$, excited at 1.0 eV and probed at 3.1 eV. Feature I corresponds to photodetachment from the excited state, while II from the ground state – see Fig. 6(b) for details. The concomitant decay of excited state signal with growth in ground state signal indicates that internal conversion is observed. (Reproduced from ref. 20 with permission. Copyright 2004 American Association for the Advancement of Science.)

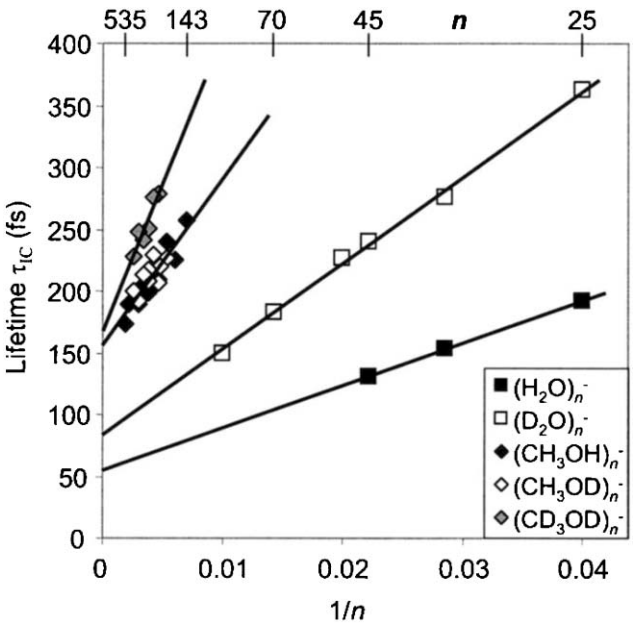

Fig. 8 Plot of the internal conversion lifetime of the excited state of $(H_2O)_n^-$ and $(MeOH)_n^-$ with $1/n$, where n is the number of solvent molecules in the cluster. Different isotopomers are assigned in the legend. A linear correlation is observed and extrapolation to the bulk agrees well with the fastest timescale observed for the analogous liquid. (Reproduced from ref. 21 with permission. Copyright 2007 American Institute of Physics.)

is measured to be $\tau_{ic} \sim 400$ fs for $(D_2O)_{25}^-$. Albeit the first dynamical process observed, the timescale does not compare favourably with that of the bulk, measured to be 70 fs in liquid D_2O. However, a size dependent study reveals that the lifetime of the excited state due to internal conversion decreases linearly with $1/n$ and extrapolates to τ_{ic} for an infinite cluster – corresponding to the bulk – in agreement with the fastest timescales observed in both liquid H_2O and D_2O.[20] This trend is shown in Fig. 8 for $(D_2O)_n$ and $(H_2O)_n$ and isotopomers of $(MeOH)_n$, discussed below[21]. Recent theoretical predictions have recovered this correlation of internal conversion rate with reciprocal cluster size, based on dipolar coupling of the electronic transition with IR active vibrational modes.[22]

The second timescale considered in detail by the Zewail group was deduced from temporal changes in the ground state photoelectron spectrum following the internal conversion. This is shown in Fig. 9(a) and (b) as difference spectra, where the PE spectrum at long-time has been subtracted to accentuate the temporally evolving features.[19] The highest energy, blue-coloured part of the spectrum corresponds to the excited state dynamics and has been considered in detail above. The red-shaded spectral window corresponds to the high energy side of the ground-state detachment feature and correlates to hot, pre-solvated ground state clusters, formed immediately following internal conversion. This is expected to lead to a broadening of the photoelectron spectrum as shown in Fig. 6(b). Finally, the yellow-coloured spectral window monitors the recovery of the spectrum and is consistent with the dynamics of the red window. Fig. 9(c) shows the integrated intensity of these spectral windows (colour coded) with time. Detailed analysis of the red spectral region reveals two distinct timescales. The first of these is a 300 fs timescale, which does not change appreciably with cluster size from $n = 15$ to $n = 35$. A second, slower timescale, increases from 2 ps to 10 ps over the same size range.

The 300 fs timescale is assigned to initial solvation, τ_s, of the vibrationally hot ground state and may be attributed to a 'local' solvation (presumably first solvation shell) due to the lack of size-dependence.[19] The timescale $\tau_s \sim 300$ fs is also in excellent agreement with the second time-scale observed in the liquid water, suggesting that this size independence may be valid up to the bulk. The third, slower timescale is assigned to a more global thermalisation throughout the system, τ_r in Fig. 6(a). In a cluster environment, this is restricted due to its finite size and consequently will lead to evaporation. Evaporation can indeed be seen from ion-yield experiments.[23] Although such a process is not commensurate with the bulk, the results suggest that the third observed timescale is due to the flow of energy form the hot local solvation shell(s) to the extended water bath, resulting in a fully thermalised hydrated electron.

Despite these compelling observations and connections to the condensed-phase, there remains some ambiguity about the interpretation based on the recent observation of isomers of large $(H_2O)_n^-$ clusters.[24] These may be classed into clusters in which the electron is predominantly within a cavity surrounded by water molecules, or clusters in which the electron resides on the surface of the cluster. The former would be a correct analogue of the hydrated electron. The latter would clearly not be appropriate and the nature of the experimentally observed isomers for these large clusters remains unclear.

Similar experiments have recently also been performed on $(MeOH)_n^-$ clusters of very large size,[21] where the question of solvation motif should be more transparent and those studied in time-resolved methods have been identified with cavity states. As for water, there has been some ambiguity concerning the dynamics observed in liquid methanol and the processes observed in clusters for sizes $145 < n < 535$ revealed overall

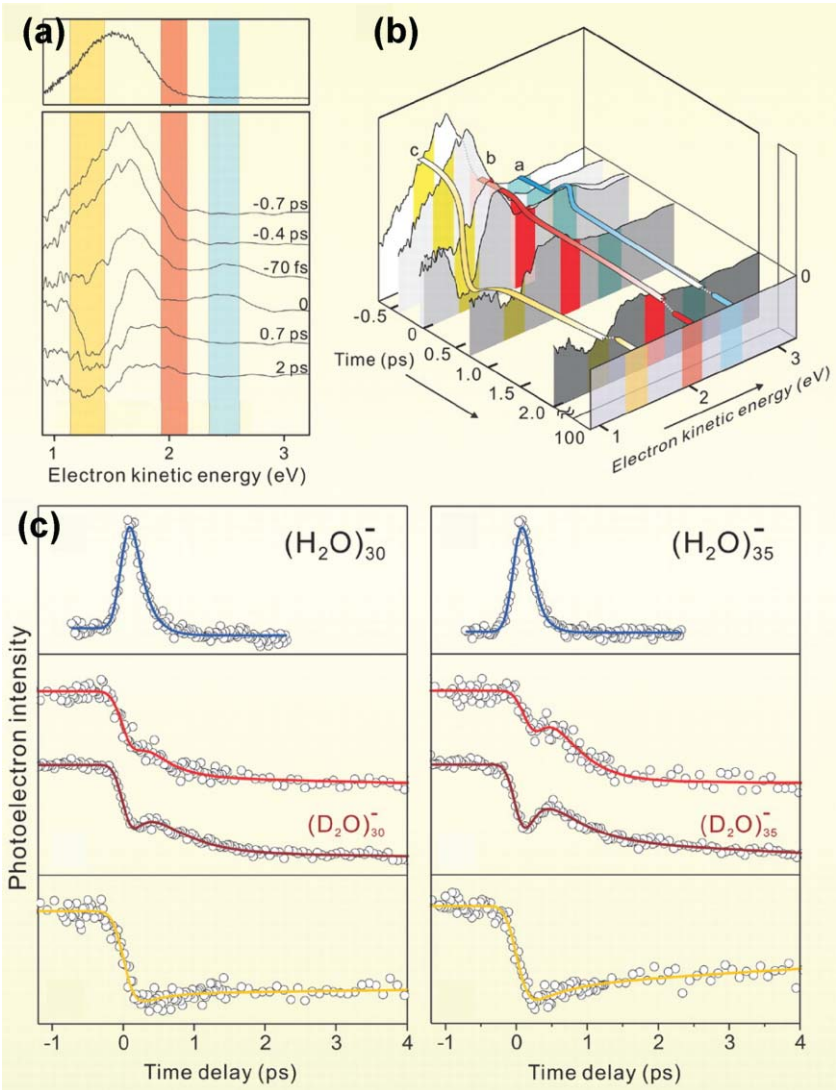

Fig. 9 (a) and (b) – time-resolved photoelectron spectra for $(H_2O)_{35}^-$, excited at 1.5 eV and probed at 3.1 eV. The top-trace in (a) is a probe-only spectrum and spectra at pump–probe delays have had a long-delay (100 ps) spectra subtracted. The blue spectral window corresponds to photo-detachment from the excited state, the red from hot, pre-solvated ground state and the yellow from fully solvated ground state – see Fig. 6 for details. (b) A three dimensional representation of the time-resolved photoelectron spectra. The integrated time-resolved intensity of the coloured spectral windows is shown in (c) for $(H_2O)_{30}^-$ and $(H_2O)_{35}^-$. (Reproduced from ref. 19 with permission. Copyright 2004 American Association for the Advancement of Science.)

similar relaxation as for $(H_2O)_n^-$ clusters. That is, the first observed mechanism could be assigned to internal conversion on a $\tau_{ic} \sim$ 170–270 fs timescale and this is followed by ground state solvation on a $\tau_s \sim$ 750 fs timescale. Although not quite as clear, a linear correlation of the timescale for internal conversion with $1/n$ is again noted and internal conversion timescales for $(MeOH)_n^-$ and different isotopomers are shown in Fig. 8. Because of the large size of these clusters, it is apparent from Fig. 8 and the $1/n$ scaling, that the primary relaxation dynamics have nearly converged to the bulk.

3.3 Electron thermalisation in metal clusters

Having discussed solvation dynamics in a few differing contexts, the next subsections discuss metal clusters. The dominant feature observed in terms of electronic structure of a metal in going from an isolated atom – through clusters and nano-particles – to the condensed-phase, is that the density-of-states (DOS) increases rapidly as the linear combinations of the atomic orbitals converge to the familiar band structure of solid-state materials. This size-dependent evolution has been extensively studied using PES of cluster anions, which indicate that the development of bands occurs even in relatively small clusters, particularly for transition metal clusters. In metals, there a continuous distribution of electrons, up to the Fermi level, above which is an equally dense distribution of unoccupied orbitals – see Fig. 10(a). Upon excitation, intra-band (and inter-band) excitations form a non-thermal electron distribution as shown in Fig. 10(b). In the condensed-phase, the relaxation that ensues involves a number of steps. Generally, the most rapid of these is the thermalisation of the electron gas through inelastic electron–electron scattering

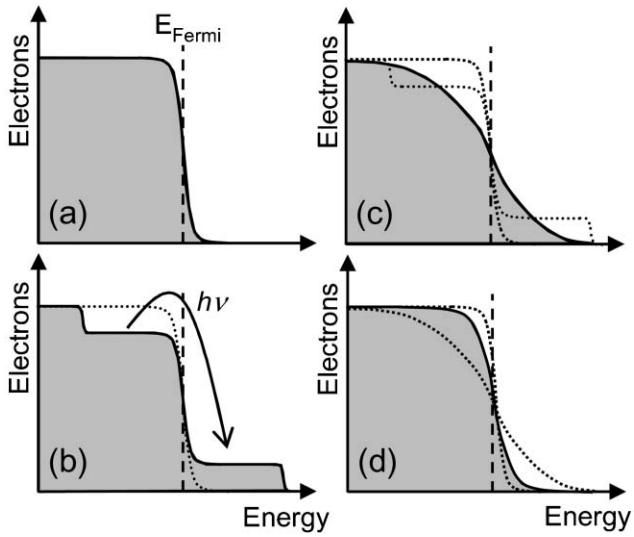

Fig. 10 Schematic representation of the relaxation dynamics of a photo-excited metal. In (a), the nascent metal has filled orbitals up to the Fermi level. Excitation creates a non-thermal electron distribution (b). The electron gas thermalises *via* electron–electron scattering (c) and then equilibrates with the surrounding lattice *via* electron–phonon coupling (d). The resultant distribution is a typical Fermi–Dirac distribution.

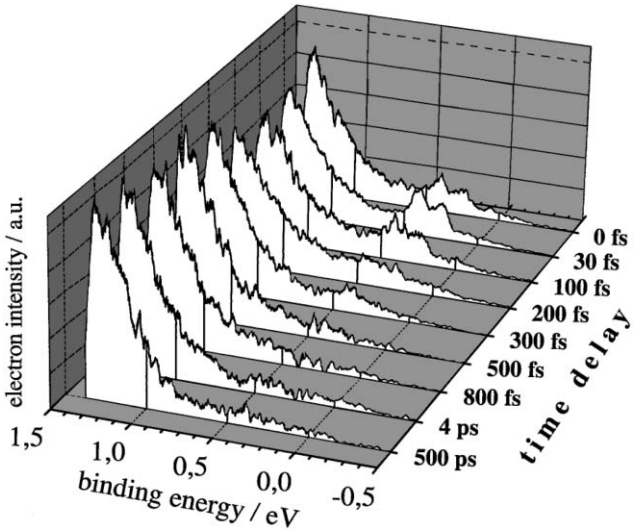

Fig. 11 Time-resolved photoelectron spectra for Pt_3^- excited and probed at 1.5 eV. The feature around 0.3 eV binding energy in the upper-most spectrum corresponds to the initially excited states. With pump–probe delay, this feature broadens and shifts. The observed excited state dynamics correlate to very fast electron–electron scattering. (Reproduced from ref. 27 with permission. Copyright 2000 The American Physical Society.)

leading to a hot distribution around the Fermi level, Fig. 10(c). This inelastic scattering process is very efficient and typically occurs on a $\tau_{e-e} < 100$ fs timescale. Following this electronic thermalisation, the effective electron temperature can be several hundred degrees higher than that of the lattice and the electronic energy is dissipated through electron–phonon coupling and ultimately dispersed around the whole system, resulting in a thermally equilibrated state, Fig. 10(d).

In a series of papers, the Eberhardt group presented a comprehensive study of some of the above-mentioned processes in transition metal clusters: Ni_n^-, Pd_n^-, and Pt_n^- using TRPES.[25–27] Using a 1.5 eV pump pulse, the non-thermal distribution was generated and the subsequent dynamics monitored by probe pulses at 1.5 eV or 3.0 eV. The resulting photoelectron spectra are shown for Pt_3^- in Fig. 11.[27] The double peak observed at $\sim$0.2 eV binding energy corresponds to photoemission from the initially excited clusters. As time elapses, this feature is observed to broaden rapidly and shift towards higher binding energy. The lifetime extracted from the intensity of this feature with time and the known temporal resolution ($\sim$275 fs), yields $\tau_{e-e} < 70$ fs. The broadening and lifetime are consistent with efficient electron–electron scattering as the non-thermal electron distribution is thermalised. These extremely high rates imply that clusters of very few atoms can exhibit bulk dynamics and suggest that there is a sufficiently high DOS for the Auger-like scattering to occur.

Similarly fast timescales for excited state relaxation were observed in Pd_n^- clusters, where τ_{e-e} ranges from: $\tau_{e-e} \sim 42$ fs for $n = 3$, to $\tau_{e-e} \sim 91$ fs for $n = 4$, and $\tau_{e-e} \sim 25$ fs for $n = 7$.[26] The distribution of timescales highlights that the incremental increase in size of the cluster has an effect and suggests that the band, albeit dense, is still rather granular. For very large clusters, such effects should become less noticeable as the 'molecular' nature converges to the bulk, where the timescale for this process is 10 fs.

For Ni_3^- and Pd_n^- clusters, a second slower timescale could also be identified and was attributed to electronic energy transfer into the vibrational modes of the cluster – analogous to electron–phonon coupling.[25,26] On a small-cluster scale, phonons are not well-defined and the dynamics are best described as a series of internal conversions, which results in the dissipation of electronic energy into the vibronic modes of the cluster. The timescale in Pd_4^- and Pd_7^- for this process is observed to be 700 fs and 1 ps, respectively. These timescales are again consistent with those observed in the bulk and in general the *d*-metal clusters behave very much like their bulk counterpart.

Complementary to these studies, the Ganteför group considered a range of metallic clusters in which the DOS is lower around the Fermi level, with the anticipation that the dynamics observed should differ substantially as inelastic scattering is inhibited. This is indeed the case for Au_n^- clusters, which show excited state lifetimes of 1.2 ns for Au_3^- and 500 ps for Au_6^- following excitation at 1.5 eV.[28] In stark contrast, Al_n^- clusters with $6 \leqslant n \leqslant 15$ and Ag_n^- clusters with $3 \leqslant n \leqslant 21$, show a much more rapid relaxation, ranging between $\sim$200 fs and 500 fs for Al_n^- [29] and between $<$110 fs and 630 fs for Ag_n^-, with the exception of Ag_7^-, whose excited state relaxes with a time constant of 3.8 ps.[30]

Fig. 12 show observed dynamics of Al_{10}^-, a representative Al_n^- cluster, where the top trace shows the single-photon photoelectron spectrum for this cluster. The left column shows the dynamics following excitation at 1.55 eV at various delays, scaled vertically to highlight the dynamics, while the right column show the difference spectra to further accentuate time-resolved features. With delay, a gradual shift and broadening

towards lower eKE (higher binding energy) is observed and is similar in appearance to dynamics seen for the *d*-metal clusters. In contrast, the time-resolved photoelectron spectra of Au_3^- and Au_6^- shows a well-defined peak, which gradually disappears with time. The contrasting dynamics observed for Al_n^- and Ag_n^- with respect to Au_n^- has in part been attributed to the nature of the intermolecular bonding. For Al_n^- and Ag_n^- clusters, this is rather 'floppy' and shape deformations are easily induced.[29,30] In contrast, small Au_n^- clusters are rigid because of strong relativistic effects leading to *sd* hybridisation and a reduced internuclear bond distance. This difference can in part account for the observed timescale variation – Al_n^- and Ag_n^- clusters have large density of vibrational states to which the electronically excited states couple, leading to fast internal conversion. However, the strong bonding in Au also results in larger energy gaps between the molecular orbitals. As a consequence, there is also a reduced density of electronic states, lowering the rate of electron–electron scattering. The dynamics observed in Fig. 12 for Al_{10}^- are consistent with both electron–electron scattering and electron–vibration coupling and for both Al_n^- and Ag_n^-, it is not immediately clear which of the two processes dominates.

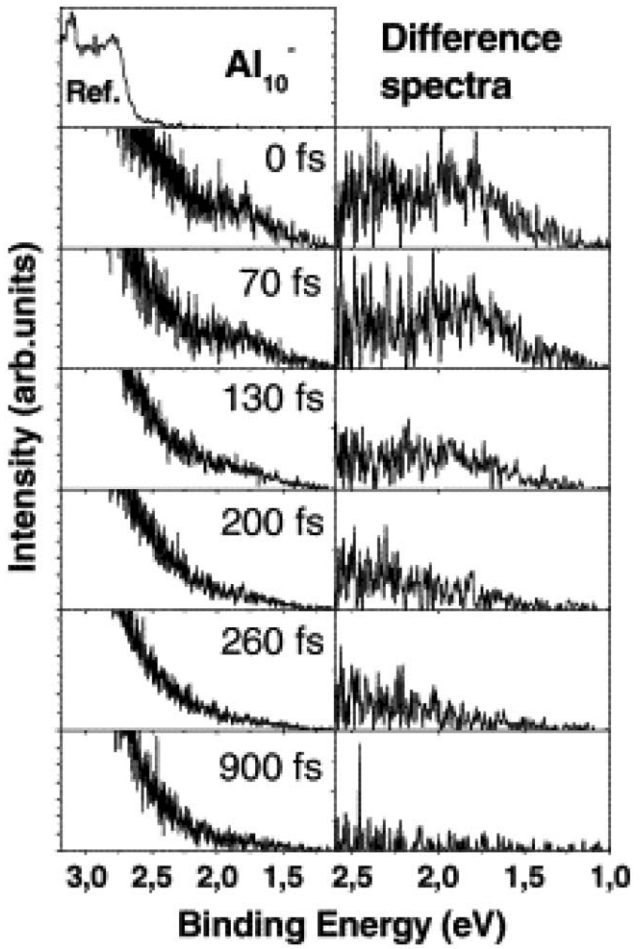

Fig. 12 Time-resolved photoelectron spectra for Al_{10}^- excited at 1.55 eV and probed at 3.1 eV. The top left trace is the photoelectron spectrum of Al_{10}^- as a reference. Time-resolved spectra at various delay times are shown on the left. The right column is the same data with a spectrum at very long delay subtracted to accentuate the time-dependent signal. As time elapses, the excited state distribution can be seen to shift towards higher binding energy and reduce in intensity. (Reproduced from ref. 28 with permission. Copyright 2003 Elsevier B. V.)

The extreme case of electron–vibrational coupling can be observed in Hg_n^- clusters.[31,32] These are characterised by a band-gap separating the full *s*-band from the *p*-band, which is singly occupied in the anion. If the excitation energy is less than this band-gap, intra-band excitation results in a *single* excited electron in the otherwise empty *p*-band. Inelastic electron scattering is energetically forbidden. In general, the initial excited state decays between 6 and 14 ps for clusters in the range $7 \leqslant n \leqslant 18$. The dynamics are interpreted and modelled using a simple molecular picture of a series of internal conversion events, which leads to spectral shifting and broadening.[32] Like Al_n^- and Ag_n^-, Hg_n^- clusters are flexible and are predominantly van der Waals bound for small clusters due to their closed shell atomic structure. As a result, internal conversion may be expected to be fast. However, the dynamics are generally slower than those of Al_n^- and Ag_n^-, indicative of the additional role that inelastic electron scattering may play for these clusters.

By studying a range of metallic clusters with a range of differing band structures, these complementary experiments demonstrate that indeed, dynamics normally associated with solid-state physics can not only be seen in clusters but can also be understood on a molecular level. However, they also show that molecular effects have not converged to the bulk and the addition of single atoms can alter the dynamics quite dramatically.

3.4 Molecular desorption dynamics on cluster surfaces

In the above examples, a correlation can be drawn between a condensed phase medium and its cluster analogue. Clusters can also be considered as surfaces due to the large fraction of the constituent atoms or molecules that reside on the cluster surface, even for very large clusters. Surfaces are of immense importance in various branches of chemistry such as catalysis and a substantial amount of effort has been devoted to understanding the numerous processes operative using ultrafast methods. Of particular interest are metal substrates binding an absorbate. Photo-excitation leads to the formation of a hot electron distribution, similar to that discussed in Section 3.3 – see Fig. 10. Because electron–electron scattering rates are typically very fast (<100 fs), the primary event most commonly involves thermalisation of this unequilibrated electron gas and subsequent electron–vibrational coupling forming a hot Fermi–Dirac distribution. Energy is then transferred to the dissociative mode of the absorbate either through nonabiabatic electronic substrate–absorbate coupling or indirectly *via* thermalisation of the absorbate with the substrate. In either case, photo-induced reaction or desorption from the surface is a statistical process and typically occurs on a picosecond timescale. In competition with this is energy dissipation into the surrounding substrate, resulting in a much reduced overall reactive yield. Such dissipation channels are not present in clusters and thus, they present excellent candidates to investigate the ultrafast dynamics of surface reactivity.

Indeed, the reactivity and catalytic activity of clusters has been studied by a number of groups using mass-spectrometric methods. A particularly elegant demonstration of this is a combined experimental and theoretical study revealing the kinetic, mechanistic and structural details of the catalytic cycle for CO oxidation on a Au_2^- cluster in the presence of molecular oxygen.[33]

The group of Eberhardt investigated the dynamics of $Au_2(CO)^-$ and $Pt_2(CO)_5^-$, in which desorption of the absorbate in the former will leave a bare Au_2^- cluster while, for the latter, will react from a saturated to unsaturated Pt-carbonyl cluster.[34] Fig. 13 shows the dynamics following excitation at 1.5 eV and probing at 3.1 eV for $Au_2(CO)^-$. Compared to the probe-only spectrum, a broad distribution at low binding energy near time zero can be identified with hot electron dynamics. The highest energy (lowest binding energy) portion of the spectrum disappears on a $\sim$65 fs timescale typical of electron–electron inelastic scattering. The depletion of intensity over the region 0–1 eV proceeds on a $\sim$130 fs timescale and is assigned to the electron–vibrational coupling. As this spectral feature evolves, a sharp peak around 2 eV binding energy can be identified. This arises from photo-detachment of bare Au_2^-, as revealed by the bottom trace in Fig. 13. The appearance of Au_2^- necessitates desorption of the carbonyl group. Based on the arguments that this feature does not show any temporal evolution other than an intensity increase and that preceding hot-electron dynamics are clearly distinguishable, the authors conclude that desorption is indeed stochastic and occurs on a timescale of $\sim$500 fs. For $Pt_2(CO)_5^-$, a similar sequence of events are observed with very rapid $<$100 fs thermalisation followed by a much slower, $\sim$3 ps desorption to yield $Pt_2(CO)_4^-$. Based on molecular intuition, the reduced rate for desorption can be attributed to the larger number of degrees of freedom throughout which energy can be distributed.[34]

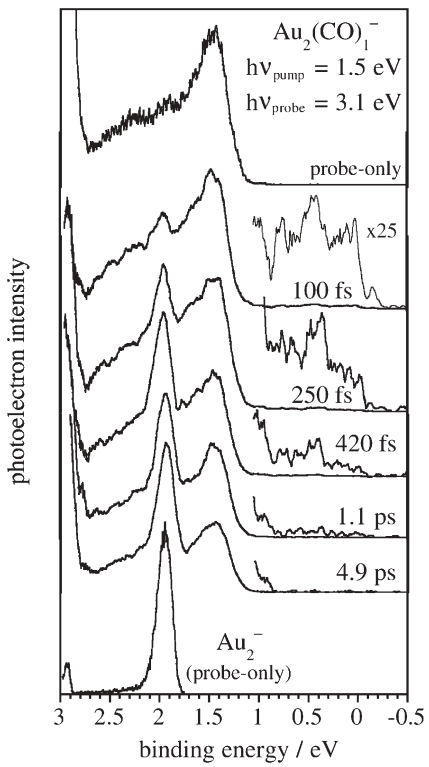

Fig. 13 Time-resolved photoelectron spectra for $Au_2(CO)^-$ excited at 1.5 eV and probed at 3.0 eV. The top trace is a probe-only spectrum of $Au_2(CO)^-$, while the bottom trace is a probe-only spectrum of Au_2^-. Pump–probe delays are indicated on the traces. The feature between 0–1 eV binding energy corresponds to the initially excited states. This is observed to deplete rapidly, while a new feature appears at 2 eV binding energy, which is assigned to photo-detachment of Au_2^-. The observation of Au_2^- indicates that CO has undergone desorption. (Reproduced from ref. 34 with permission. Copyright 2002 The American Physical Society.)

In both these cases, desorption is clearly observed to be thermal, in accord with the most common mode of desorption from an extended surface. However, a unique property of clusters is that they can also provide properties which are normally not associated with bulk dynamics. An example of this in terms of surface chemistry was shown by the Ganteför group, which probed the *direct* photo-desorption from $Ag_n(O_2)^-$ clusters.[35] Direct photo-desorption is unlikely in the bulk because a dissociative–excited state accessed is quenched by rapid energy redistribution. As argued in the previous sub-section, clusters of simple metals generally have reduced electron–electron scattering rates due to a lower DOS and may thus be expected to have excited lifetimes sufficiently long to allow competitive direct desorption.

Time-resolved photoelectron spectra for even-numbered $Ag_nO_2^-$ clusters are shown in Fig. 14. From this, the assignment to direct photo-desorption is based on the analysis of the $Ag_2O_2^-$ spectra. At time zero, an intense photoelectron feature at high eKE is observed and is composed of a series of peaks. For $Ag_2O_2^-$, these are correlated to the vibrational energy levels of Ag_2 binding the O_2 molecule in the neutral, which are accessed by photo-detachment of the anion. In $Ag_4O_2^-$ and $Ag_8O_2^-$, this splitting is somewhat larger and is more comparable to the vibrational splitting in O_2^+, which may indicate some charge transfer. Nevertheless, the observation is an indication of the binding of the O_2 unit to the Ag_2 'surface'. The feature at 0.6 eV, seen at long time-delay in the $Ag_2O_2^-$ spectra, is from the photo-detachment of bare Ag_2^-. For $Ag_4^-$and Ag_8^-, the electron affinity exceeds the photon energy of the probe and thus, the analogous features are not seen in spectra of $Ag_4O_2^-$ and $Ag_8O_2^-$. Analysis of the changes in the photoelectron spectral shape, observed with pump–probe delay, indicate a direct rather than statistical desorption. This is further supported by the very fast desorption dynamics of $<$100 fs. The general similarity of the $Ag_4O_2^-$ and $Ag_8O_2^-$ dynamics suggests a similar direct process for these. In contrast, lifetimes for $Ag_3O_2^-$ are observed to be 5.4 ps and do not show the spectral signatures or evolution present in the even-numbered clusters. It was speculated that this can be consolidated by the fact that atomic oxygen was used to generate these clusters such that two unbound oxygen atoms could be chemisorbed onto the Ag_3^- cluster.[35]

4. Summary and outlook

Time-resolved methods, and specifically TRPES, provide powerful insight into ultrafast processes on a molecular level.

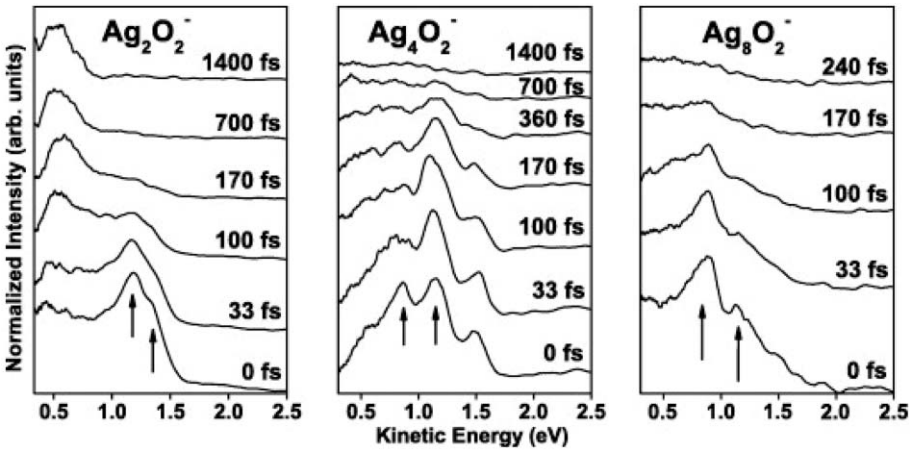

Fig. 14 Time-resolved photoelectron spectra for, from left to right: $Ag_2(O_2)^-$, $Ag_4(O_2)^-$, and $Ag_8(O_2)^-$, excited at 3.1 eV and probed at 1.55 eV. The broad feature at 0 fs delay corresponds to the initially excited state. This is observed to decay and for $Ag_2(O_2)^-$, the feature at 0.6 eV corresponds to photo-detachment of Ag_2^-. Upward arrows indicate fine structure due to O_2 stretching vibrations excited in the neutral, following photo-detachment by the probe pulse. (Reproduced from ref. 35 with permission. Copyright 2007 Elsevier B. V.)

When applied to mass-selected cluster anions, such insights may be related directly to condensed-phase systems by performing size-dependent studies. Even at surprisingly small sizes, phenomena normally associated with the condensed phase can be observed and, in some cases, directly compared to their bulk analogue. As part of 'approaching the bulk', size matters. By performing experiments on ever larger cluster, the connection promises to become more pronounced. To this end, recent time-resolved experiments on $(MeOH)_n^-$ with clusters exceeding 500 methanol molecules demonstrate that ultrafast dynamics in truly nano-sized systems can be measured in the gas-phase. However, any extrapolation from the gas- to the condensed-phase must be done with great care as clusters retain many 'molecular' characteristics, some of which have no bulk analogue. Nevertheless, it is also this molecularity that gleans much insight into bulk dynamics on the atomic scale.

Although a relatively young field, TRPES on cluster anions and anionic molecules is developing rapidly and diverging into new and exciting areas of research. For example, the Zewail group recently studied relaxation dynamics following excitation of the active chromophore of the photo-active yellow protein using TRPES.[36] The study of biologically relevant systems using these techniques promises to provide a molecular understanding of the primary events in extended bio-cycles. Soft ionisation techniques such as atmospheric pressure ionisation and matrix-assisted laser-desorption ionisation (MALDI) hold substantial promise in this regard as they provide the ability to produce very large and fragile species in the gas-phase as demonstrated in countless mass-spectrometry laboratories. The Wang group has demonstrated that PES can be coupled to such sources[37] and the Kappes group has recently demonstrated the first TRPES measurements using electrospray ionisation to generate the C_{60}^- cluster.[38] Experiments of this nature are currently underway in our laboratory, with specific interest in the dynamics of inorganic clusters and bio-active anions. In addition to the incorporation of new cluster sources, new laser sources can also probe dynamics that were hitherto unexplored. Sub-50 fs time-resolution will allow one to investigate the most rapid of processes, such as dynamics through conical intersections, whereas picosecond TRPES provides enhanced spectral resolution and could probe subtle vibrational relaxation dynamics. This has been demonstrated in neutrals where internal vibrational relaxation can be monitored in detail.

Acknowledgements

I would like to thank D. M. Neumark and V. G. Stavros for proofreading the manuscript and useful suggestions. Financial support is provided by the EPSRC under grant EP/D073472/1

References

1 A. W. Castleman and K. H. Bowen, *J. Phys. Chem.*, 1996, **100**, 12911.
2 A. H. Zewail, *J. Phys. Chem. A*, 2000, **104**, 5660.
3 A. Stolow, A. E. Bragg and D. M. Neumark, *Chem. Rev.*, 2004, **104**, 1719.
4 T. E. Dermota, Q. Zhong and A. W. Castleman, *Chem. Rev.*, 2004, **104**, 1861.
5 W. C. Wiley and I. H. McLaren, *Rev. Sci. Instrum.*, 1955, **26**, 1150.
6 P. Kruit and F. H. Read, *J. Phys. E: Sci. Instrum.*, 1983, **16**, 313.
7 A. Eppink and D. H. Parker, *Rev. Sci. Instrum.*, 1997, **68**, 3477.
8 R. Mabbs, K. Pichugin and A. Sanov, *J. Chem. Phys.*, 2005, **123**, 054329.
9 T. Suzuki, *Annu. Rev. Phys. Chem.*, 2006, **57**, 555.
10 A. L. Harris, J. K. Brown and C. B. Harris, *Annu. Rev. Phys. Chem.*, 1988, **39**, 341.
11 A. Sanov and W. C. Lineberger, *Phys. Chem. Chem. Phys.*, 2004, **6**, 2018 and references therein.
12 V. Vorsa, S. Nandi, P. J. Campagnola, M. Larsson and W. C. Lineberger, *J. Chem. Phys.*, 1997, **106**, 1402.
13 B. J. Greenblatt, M. T. Zanni and D. M. Neumark, *J. Chem. Phys.*, 1999, **111**, 10566.
14 B. J. Greenblatt, M. T. Zanni and D. M. Neumark, *J. Chem. Phys.*, 2000, **112**, 601.
15 A. V. Davis, R. Wester, A. E. Bragg and D. M. Neumark, *J. Chem. Phys.*, 2003, **119**, 2020.
16 L. Kevan, *Acc. Chem. Res.*, 1981, **14**, 138.
17 M. S. Pshenichnikov, A. Baltuska and D. A. Wiersma, in *Few-Cycle Laser Pulse Generation and Its Applications*, *Topics in Applied Physics*, Springe-Verlag, Berlin & Heidelberg, 2004, vol. 95, pp. 409–444, and references therein.

18 J. M. Weber, J. Kim, E. A. Woronowicz, G. H. Weddle, I. Becker, O. Cheshnovsky and M. A. Johnson, *Chem. Phys. Lett.*, 2001, **339**, 337.
19 D. H. Paik, I. R. Lee, D. S. Yang, J. S. Baskin and A. H. Zewail, *Science*, 2004, **306**, 672.
20 A. E. Bragg, J. R. R. Verlet, A. Kammrath, O. Cheshnovsky and D. M. Neumark, *Science*, 2004, **306**, 669.
21 A. Kammrath, G. B. Griffin, J. R. R. Verlet, R. M. Young and D. M. Neumark, *J. Chem. Phys.*, 2007, **126**, 244306.
22 S. F. Fischer and W. Dietz, *Z. Phys. Chem.*, 2007, **221**, 1.
23 P. J. Campagnola, L. A. Posey and M. A. Johnson, *J. Chem. Phys.*, 1991, **95**, 7998.
24 J. R. R. Verlet, A. E. Bragg, A. Kammrath, O. Cheshnovsky and D. M. Neumark, *Science*, 2005, **307**, 93.
25 N. Pontius, M. Neeb, W. Eberhardt, G. Luttgens and P. S. Bechthold, *Phys. Rev. B: Condens. Matter Mater. Phys.*, 2003, **67**, 035425.
26 N. Pontius, G. Luttgens, P. S. Bechthold, M. Neeb and W. Eberhardt, *J. Chem. Phys.*, 2001, **115**, 10479.
27 N. Pontius, P. S. Bechthold, M. Neeb and W. Eberhardt, *Phys. Rev. Lett.*, 2000, **84**, 1132.
28 M. Niemietz, P. Gerhardt, G. Ganteför and Y. D. Kim, *Chem. Phys. Lett.*, 2003, **380**, 99.
29 P. Gerhardt, M. Niemietz, Y. D. Kim and G. Ganteför, *Chem. Phys. Lett.*, 2003, **382**, 454.
30 M. Niemietz, M. Engelke, Y. D. Kim and G. Ganteför, *Phys. Rev. B: Condens. Matter Mater. Phys.*, 2007, 75.
31 A. E. Bragg, J. R. R. Verlet, A. Kammrath, O. Cheshnovsky and D. M. Neumark, *J. Chem. Phys.*, 2005, **122**, 054314.
32 J. R. R. Verlet, A. E. Bragg, A. Kammrath, O. Cheshnovsky and D. M. Neumark, *J. Chem. Phys.*, 2004, **121**, 10015–10025.
33 L. D. Socaciu, J. Hagen, T. M. Bernhardt, L. Woste, U. Heiz, H. Hakkinen and U. Landman, *J. Am. Chem. Soc.*, 2003, **125**, 10437–10445.
34 G. Luttgens, N. Pontius, P. S. Bechthold, M. Neeb and W. Eberhardt, *Phys. Rev. Lett.*, 2002, **88**, 076102.
35 M. Niemietz, K. Koyasu, G. Ganteför and Y. D. Kim, *Chem. Phys. Lett.*, 2007, **438**, 263.
36 I. R. Lee, W. Lee and A. H. Zewail, *Proc. Natl. Acad. Sci. U. S. A.*, 2006, **103**, 258.
37 L. S. Wang, C. F. Ding, X. B. Wang and S. E. Barlow, *Rev. Sci. Instrum.*, 1999, **70**, 1957.
38 O. T. Ehrler, J. P. Yang, C. Hattig, A. N. Unterreiner, H. Hippler and M. M. Kappes, *J. Chem. Phys.*, 2006, **125**, 074312.